

# Emission angle dependent pion interferometry at RHIC and beyond

Ulrich Heinz<sup>1,2</sup> and Peter F. Kolb<sup>2,3</sup>

<sup>1</sup>*Physics Department, The Ohio State University, Columbus, OH 43210*

<sup>2</sup>*Kavli Institute for Theoretical Physics, University of California, Santa Barbara, CA 93106-4030*

<sup>3</sup>*Department of Physics and Astronomy, State University of New York, Stony Brook, NY 11794-3800*

(Dated: July 10, 2002 (revised version))

We use hydrodynamics to generate freeze-out configurations for non-central heavy-ion collisions at present and future collider energies. Such collisions are known to produce strong elliptic flow. The accompanying space-time structure of the source at freeze-out is analyzed using pion interferometry. Between RHIC and LHC energies the source deformation in the transverse plane changes sign. This leaves characteristic signatures in the emission angle dependence of the HBT radii.

PACS numbers: 25.75.-q, 25.75.Gz, 24.10.Nz

Heavy-ion collision data from the Relativistic Heavy Ion Collider (RHIC) [1] have produced strong indications for a large degree of thermalization in these collisions. Only dynamical models with very intense reinteractions among the produced particles [2, 3, 4], in particular the hydrodynamic model [5, 6, 7, 8, 9, 10, 11], have been able to reproduce the large observed elliptic flow signals [12, 13, 14, 15] together with the measured systematics of the shapes of the single-particle hadron spectra [16, 17] which require strong radial flow [18]. When compared to the data, all models seem to fail which are not able to achieve almost complete local thermalization very quickly, at most 1 fm/c after nuclear impact [19, 20]. At this early time the energy density in the reaction zone is still far above 1 GeV/fm<sup>3</sup> [7], the critical value for color deconfinement, so that the thermalized state formed early in the collision has most likely been a quark-gluon plasma [20].

Even though the microscopic mechanisms causing the fast thermalization are presently not understood, these observations provide strong phenomenological support for the hydrodynamical model as a dynamical description for the space-time evolution of the reaction zone. We will therefore use it here to study additional aspects of the collision. We will concentrate in particular on the question how the strong elliptic flow affects the spatial matter distribution at “freeze-out” when the observed hadrons decouple from the fireball. Elliptic flow requires an initial spatial deformation of the nuclear overlap region in the transverse plane (i.e. either a non-zero impact parameter or collisions between deformed nuclei) since it is generated by anisotropies in the pressure gradients [5, 21]. As it develops, the matter begins to expand more rapidly in the “short” direction (which for non-central collisions between spherical nuclei lies in the reaction plane). Hydrodynamics predicts [7] that, if the initial energy density is high enough and thus the time until freeze-out sufficiently long, this initial out-of-plane deformation changes sign, leading to an “in-plane extended source” (IPES) at decoupling. We show that at RHIC energies this is not yet the case [22], but that it will eventually happen at higher

collision energies (LHC or beyond). In this paper we discuss how this transition can be probed by two-particle interferometry, in particular by studying the emission angle dependence relative to the reaction plane of the size parameters (“HBT radii”) extracted from Bose-Einstein correlation functions [23, 24, 25, 26, 27]. We show that the spatial and momentum anisotropies of the phase-space distribution at freeze-out (the *emission function*  $S(x, K)$ ) generate characteristic azimuthal oscillations of the HBT radii whose phases and amplitudes reflect this transition. The way in which they reflect it turns out to be non-trivial and will be discussed in some detail.

The hydrodynamic model and equation of state used in our calculations are described elsewhere [7]. We here study semicentral Au+Au collisions at impact parameter  $b=7$  fm.  $\mathbf{b}$  is taken to point in  $x$  direction,  $z$  is the beam axis such that  $(x, z)$  span the reaction plane, and  $y$  points perpendicular to it. We assume boost-invariant longitudinal expansion and concentrate on the dynamics in the transverse  $(x, y)$ -plane at  $z=0$  where the nuclei collide. We use two different sets of initial conditions. The first set (labelled “RHIC1”) corresponds to optimized values for central Au+Au collisions at  $\sqrt{s}=130$  A GeV, which also give a good description of the measured hadron spectra and elliptic flow in non-central collisions [12, 13, 14, 15, 16, 17] out to transverse momenta of about 2 GeV/c and impact parameters of about 10 fm [7, 8, 20]. The initial entropy density distribution is parametrized by a superposition of two components which scale with the number of wounded nucleons (with 75% weight) and binary nucleon-nucleon collisions (with 25% weight), respectively [28]. The corresponding peak value of the initial temperature, at the starting time  $\tau_0=0.6$  fm/c of the hydrodynamic expansion, in central ( $b=0$ ) collisions is  $T_0=340$  MeV, scaled down in semicentral collisions with the Glauber prescription described in [28]. Freeze-out is implemented with the Cooper-Frye algorithm [29] along a surface of constant temperature  $T_f=130$  MeV.

The second set of initial conditions (labelled “IPES”) uses a much higher initial temperature  $T_0=2$  GeV (at

$b=0$ ), and the hydrodynamic evolution is started at  $\tau_0 = 0.1 \text{ fm}/c$  and stopped when a freeze-out temperature  $T_f = 100 \text{ MeV}$  has been reached. Such a high initial temperature can probably not even be achieved at the LHC, and the strong transverse flow generated in this case probably causes the system to decouple already much closer to the hadronization temperature of (in our case)  $T_{\text{had}} = 164 \text{ MeV}$ . We force the system to start at such a high temperature and freeze out so low in order to give it enough time to convert the initial out-of-plane deformation into a final in-plane deformation (which is the phenomenon we want to study). Unfortunately, over large times and due to the strong radial flow numerical instabilities in the hydrodynamic code accumulate, and to keep these at a minimum we use (for IPES initial conditions only) an equation of state (EOS) without a sudden phase transition. Arguing that with these initial conditions the system anyway spends almost all of its time in the quark-gluon plasma phase, we simply use  $P = \frac{1}{3}e$ , corresponding to an ideal gas of massless quarks and gluons. After stopping the evolution at  $T_f$ , we assume that pions are emitted with this freeze-out temperature and the hydrodynamic flow established on the corresponding freeze-out surface. This implies a change of EOS at freeze-out and is thus not entirely dynamically consistent; however, since modifications of the dynamics resulting from a proper transition to a hadron resonance gas EOS at hadronization are expected to have at most minor effects on the source anisotropy at such a late time, this dynamical inconsistency should not qualitatively affect our results.

The pion emission function  $S(x, K)$  for pions of a given charge is computed from the hydrodynamic output by the Cooper-Frye prescription [29]

$$S(x, K) = \frac{1}{(2\pi)^3} \int_{\Sigma} \frac{K \cdot d^3\sigma(x') \delta^4(x-x')}{\exp[K \cdot u(x')/T_f] - 1}. \quad (1)$$

This includes only directly emitted pions. While resonance decay pions strongly affect the shape of the single-particle spectrum, the same is not true for the HBT radii extracted from the two-pion correlator [30]. They do, however, generate a non-Gaussian spatial tail in the emission function [9, 30] which significantly increases its spatial widths (“homogeneity lengths”, see [26]), thereby destroying [31] the direct correspondence between the latter and the measured HBT radii which exists for Gaussian sources [26]. Since we want to preserve this correspondence as much as possible, we exclude decay pions when calculating the homogeneity lengths. We have checked that the remaining differences between the HBT radii calculated from the homogeneity lengths (see below) and those extracted from a Gaussian fit to the correlation function (calculated in the standard way [32] by Fourier transforming the emission function) are small enough to not affect the qualitative features of our results.

In equation (1),  $\Sigma$  denotes the freeze-out surface  $t_f(x)$

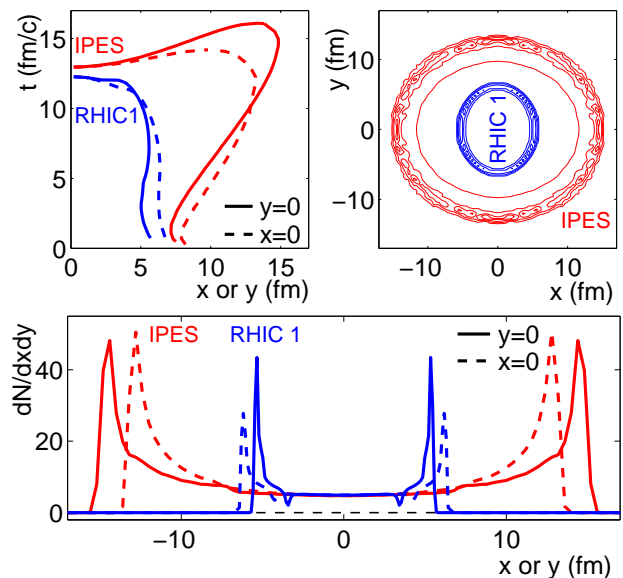


FIG. 1: (a) Cuts through the freeze-out surface  $t_f(r)$  at  $z=0$  along and perpendicular to the reaction plane. (b) Contour plots in the transverse plane of the time-,  $z$ -, and momentum-integrated emission function  $d^2N/d^2r$  for RHIC1 and IPES initial conditions (see text). (c) Cuts through diagram (b) along and perpendicular to the reaction plane, for RHIC1 and IPES initial conditions.

of constant temperature  $T_f$ , and  $u^\mu(x')$  is the flow velocity on  $\Sigma$ . Figure 1a shows cuts through  $\Sigma$  along ( $y=0$ ) and perpendicular to the reaction plane ( $x=0$ ). Initially the source is extended out-of-plane (larger in  $y$  than in  $x$  direction), but it then expands more rapidly into the  $x$ -direction, becoming in-plane elongated at later times. For RHIC1 initial conditions this only happens after most of the matter has already decoupled; as a consequence the time-integrated source, shown in Fig. 1b, is still longer in  $y$  than in  $x$  direction in the RHIC1 case. For IPES initial conditions the deformation changes sign before most particles decouple, and the time-integrated source appears in-plane-extended (see again Fig. 1b). Also, it is much larger due to the much higher initial energy density and longer lifetime.

Figure 1c shows cuts along and perpendicular to the reaction plane through the density contour plots  $d^2N/d^2r = \int (d^3K/E_K) dz dt S(x, K)$  of Fig. 1b. Pion emission is seen to be strongly surface peaked, in particular at RHIC1 where the freeze-out radius is almost constant for a long time. This “opacity” is weaker both at lower collision energies (where the freeze-out surface shrinks to zero continuously [33]) and at higher energies, due to larger temporal variations of the freeze-out radius.

Figures 2 and 3 show the spatial distributions of pions emitted with fixed momentum. Shown are density contours of  $\int dz dt S(x, K)$  in the transverse plane ( $x, y$ ) for pions with rapidity  $Y=0$  and fixed  $K_\perp$ , for three emission angles  $\Phi=0, 45^\circ$  and  $90^\circ$  relative to the reac-

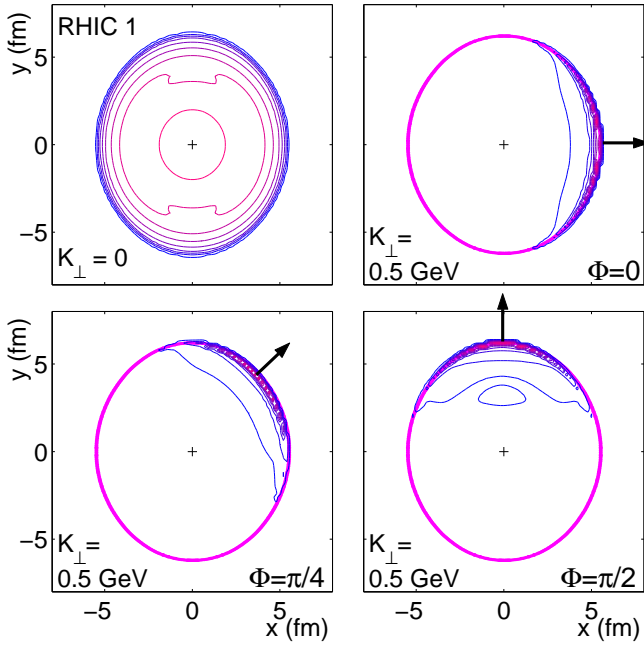


FIG. 2: Contours of constant emission density in the transverse plane for RHIC1 initial conditions (see text). The thick line indicates the largest transverse extension of the freeze-out hypersurface (see Figs. 1a,b). The four panels show emission regions for midrapidity pions ( $Y=0$ ) with  $K_{\perp}=0$  and, for three emission angles indicated by arrows, with  $K_{\perp}=0.5$  GeV.

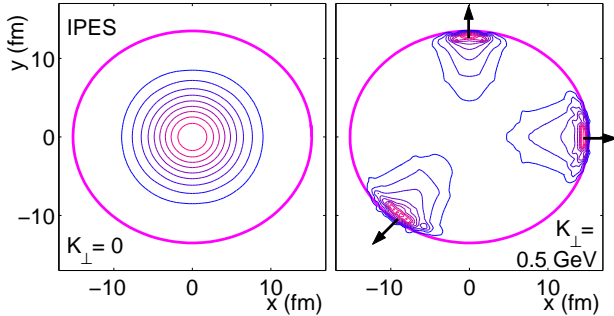


FIG. 3: Same as Fig. 2, but for IPES initial conditions.

tion plane. (In Fig. 3 we replaced  $\Phi=45^\circ$  for clarity by the equivalent angle  $\Phi=225^\circ$ .) Particles with vanishing transverse momentum  $K_{\perp}$  are seen to be emitted from almost the entire interior of the “bathtub” shown in Figs. 1b,c; for RHIC1 (IPES) initial conditions this region is elongated out-of-plane (in-plane). For slow pions the source thus looks transparent. Pions with sufficiently large transverse momenta are emitted from relatively thin regions close to the rim of the “bathtub” where the flow velocity is largest and points into the direction of the emitted pions. For fast pions the source thus looks opaque [34, 35, 36]. Their emission regions rotate with the emission angle, constrained by the shape of the “bathtub” even though they are much smaller.

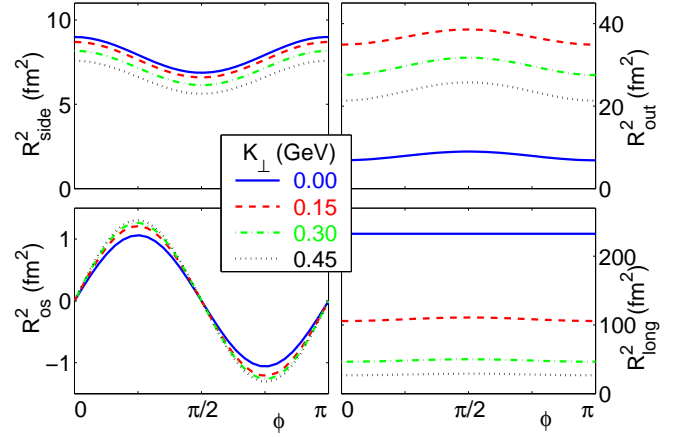


FIG. 4: Azimuthal oscillations of the HBT radii at  $Y=0$  for  $b=7$  fm Au+Au collisions at  $\sqrt{s}=130$  A GeV (RHIC1), for four values of the transverse momentum  $K_{\perp}$  as indicated.

Again we see that the opaqueness is stronger at RHIC than at higher energies. It is also seen to be anticorrelated with the curvature of the “bathtub” wall: where the curvature is large, the source is squeezed less tightly to the wall than where it is smaller. Fig. 3b shows that for IPES this geometric effect wins over the anisotropic flow effects which push the emission region more strongly towards the wall in  $x$  than in  $y$  direction; for RHIC1 both effects act together.

We now proceed to compute the HBT radii from the widths of the  $K$ -dependent emission regions [26]. The indices  $o$  (for “outward”) and  $s$  (for “sideward”) indicate the directions parallel and perpendicular to the emission vector  $\mathbf{K}_{\perp}$ ;  $l$  indicates the longitudinal  $z$  direction [26]. Given the spatial correlation tensor  $S_{\mu\nu} = \langle x_{\mu}x_{\nu} \rangle - \langle x_{\mu} \rangle \langle x_{\nu} \rangle$ , which describes the ( $K$ -dependent) widths of the emission region in space and time, the HBT radii can be calculated at midrapidity ( $Y=0$ ) from the relations [24, 25]

$$\begin{aligned}
 R_s^2 &= \frac{S_{xx}+S_{yy}}{2} - \frac{S_{xx}-S_{yy}}{2} \cos(2\Phi) - S_{xy} \sin(2\Phi), \\
 R_o^2 &= \frac{S_{xx}+S_{yy}}{2} + \frac{S_{xx}-S_{yy}}{2} \cos(2\Phi) + S_{xy} \sin(2\Phi) \\
 &\quad - 2\beta_{\perp}(S_{tx} \cos \Phi + S_{ty} \sin \Phi) + \beta_{\perp}^2 S_{tt}, \\
 R_{os}^2 &= S_{xy} \cos(2\Phi) - \frac{S_{xx}-S_{yy}}{2} \sin(2\Phi) \\
 &\quad + \beta_{\perp}(S_{tx} \sin \Phi - S_{ty} \cos \Phi). \\
 R_l^2 &= S_{zz}.
 \end{aligned} \tag{2}$$

Note that  $R_o^2$  and  $R_{os}^2$  receive purely geometric (first lines) and mixed space-time correlation contributions (second lines of the equations). Since we want to use pion interferometry to obtain information on the geometric deformation of the source at freeze-out, these must be discussed separately (see Fig. 5 below).

In addition to the explicit  $\Phi$  dependence exhibited in

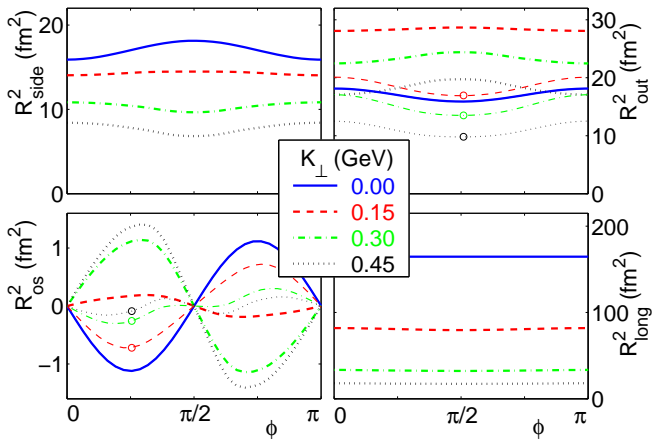


FIG. 5: Same as Fig. 4, but for IPES initial conditions. For  $R_o^2$  and  $R_{os}^2$  the geometric contributions are shown separately as thin circled lines (see text).

Eqs. (2), which arises from the angle  $\Phi$  between the  $(o, s)$  and  $(x, y)$  coordinate systems [24], the spatial correlation tensor  $S_{\mu\nu}$  depends implicitly on  $\Phi$  through the emission function  $S(x; Y, K_{\perp}, \Phi)$ . The combined  $\Phi$  dependence of the radius parameters is shown in Figs. 4 and 5, for RHIC1 and IPES initial conditions, respectively. We first note that  $R_l^2$  does not show any interesting azimuthal oscillations and requires no further discussion. The same turns out to be true for the emission duration  $S_{tt}$  (the last term contributing to  $R_o^2$  in Eqs. (2)). Interesting temporal contributions to the oscillation patterns of  $R_o^2$  and  $R_{os}^2$  thus only involve the terms  $S_{tx}$  and  $S_{ty}$  which correlate the freeze-out positions with time.

Let us first discuss the geometric contributions. From Figs. 2 and 3 we already know that pions with  $K_{\perp} = 0$  are emitted from almost the entire fireball and thus probe the different sign of the spatial deformation of the *total* (momentum-integrated) RHIC1 and IPES sources shown in Fig. 1. This is reflected by the opposite sign of the oscillation amplitudes of  $R_s^2$  and of the geometric contribution to  $R_o^2$  in Figs. 4 and 5 at  $K_{\perp} = 0$ . (For clarity we do not show separately the purely geometric contributions to  $R_o^2$  and  $R_{os}^2$  in Fig. 4 because at RHIC1 they oscillate in the same way as the total radii, in contrast to the IPES case, Fig 5.) At higher  $K_{\perp}$ -values the oscillations in Fig. 5 for  $R_s^2$  change sign, but those of the geometric contribution to  $R_o^2$  do not. This reflects an intricate interplay between geometric and flow effects, including the already mentioned weaker opacity for IPES.

The geometric contribution to the azimuthal oscillation of  $R_{os}^2$  has an interesting intuitive interpretation: Figs. 2 and 3 show that for  $K_{\perp} \neq 0$  the emission region rotates together with the emission direction  $\Phi$ , but not quite in phase. For each direction  $\Phi$  we can diagonalize the spatial correlation tensor in the transverse plane. Let us denote the major axes by  $X$  and  $Y$ , with  $X$  pointing

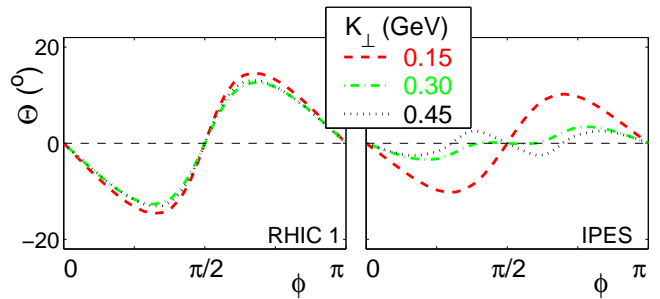


FIG. 6: The tilt angle  $\Theta$  of the major axes of the emission region in the transverse plane relative to the  $(o, s)$  system, for different values of  $K_{\perp}$ .

approximately outward and  $Y$  approximately parallel to the fireball surface. It is then easy to show that

$$R_{os}^{2(\text{geom})} = \frac{1}{2}(S_{XX} - S_{YY}) \sin(2\Theta), \quad (3)$$

where  $\Theta$  is the tilt angle between the outward-pointing major axis  $X$  and the emission direction  $\mathbf{K}_{\perp}$  (resp. the direction of  $x_o$ ). Positive values of  $\Theta$  correspond to counterclockwise rotation. Figs. 2 and 3 show that for  $K_{\perp} \neq 0$  the deformation  $\frac{1}{2}(S_{XX} - S_{YY})$  of the emission region in its major axis frame is negative for RHIC1 but positive for IPES. For RHIC1  $R_{os}^2$  is always positive in the first quadrant, while for IPES it is mostly negative. According to Eq. (3) the tilt angle  $\Theta$  is then negative in both cases, i.e. in the first quadrant the major axes  $(X, Y)$  of the emission region are always rotated clockwise against the  $(o, s)$  axes. This is confirmed by visual inspection of Figs. 2 and 3. Figure 6 shows the tilt angle  $\Theta$  as a function of the emission direction  $\Phi$ , for various values of  $K_{\perp}$ . The case  $K_{\perp} = 0$  is special since the corresponding source is  $\Phi$ -independent. Then the tilt angle is exactly  $\Theta = -\Phi \pmod{\pi}$ .

Last but not least we consider the contributions from the space-time correlations  $S_{tx}$  and  $S_{ty}$  to the oscillation amplitudes of  $R_o^2$  and  $R_{os}^2$ . They are multiplied by  $\beta_{\perp}$  (see Eqs. (2)) and thus grow with increasing  $K_{\perp}$ . They reflect the change (caused by the elliptic flow) of the spatial source deformation with increasing time. Consequently their sign does not change from RHIC1 to IPES, contrary to the spatial contributions to the oscillations. For RHIC1 they reinforce the geometric oscillations of  $R_o^2$  and  $R_{os}^2$ , but Fig. 5 shows that in the IPES case they act against them and are responsible for changing the sign of the oscillations for  $K_{\perp} \gtrsim 100 - 150$  MeV. We interpret this change of sign of the oscillations with increasing  $K_{\perp}$  as a possible experimental signature for the *spatial* manifestation of elliptic flow, i.e. the fact that the source expands faster in the  $x$  than in the  $y$  direction.

*Summary.* We have presented a detailed analysis of the space-time geometry of non-central relativistic heavy ion collisions within an ideal hydrodynamic framework. Although the idealized hydrodynamic picture with Cooper-

Frye freeze-out does not [20] give a quantitative description of the experimental HBT radii for central Au+Au collisions at RHIC [37] and should eventually be replaced by a more realistic approach to kinetic freeze-out [6, 9, 10], we expect the qualitative geometric features of non-central collisions discussed here and their manifestation in the emission angle dependence of the HBT radii to be insensitive to details of how the particles decouple from the fireball. We have shown that at high enough collision energies the anisotropic flow will lead to a source which in a transverse cut is elongated along the reaction plane, orthogonal to the initial out-of-plane elongation of nuclear overlap region. As an unambiguous signature for this change of spatial deformation we identified a sign change of the oscillation amplitude as a function of emission angle of the sideward HBT radius  $R_s$  at small transverse momentum  $K_\perp$ . Along with this we point out additional changes in the oscillation patterns of  $R_o$  and  $R_{os}^2$  which are caused by a combination of geometric spatial and temporal aspects of the source at freeze-out. A sign change as a function of increasing  $K_\perp$  in the oscillations of  $R_{os}^2$  at high collision energies has been interpreted as measurable evidence for the faster growth of the source along the reaction plane than perpendicular to it, due to elliptic flow. According to our calculations the effective source at RHIC energies should still be elongated out of the reaction plane at freeze-out. The corresponding predicted oscillation pattern of the HBT observables shown in Fig. 4 is in qualitative agreement with preliminary data from RHIC [38]. Qualitatively similar conclusions as to the sign of the source deformation at RHIC have been drawn by Lisa and Wells [39], using a hydrodynamically motivated exploding source model to fit the spectra [16] and HBT radii [37, 38].

*Acknowledgments:* This work was supported in part by the U.S. Department of Energy under Contracts No. DE-FG02-01ER41190 and DE-FG02-88ER40388 and by the National Science Foundation under Grant No. PHY99-07949. We gratefully acknowledge the warm hospitality of the Kavli Institute for Theoretical Physics at the University of Santa Barbara during the Workshop Program “QCD in the RHIC Era”.

---

[1] Proceedings of “Quark Matter 2001”, T.H. Hallmann et al. (eds.), Nucl. Phys. A **698**, 1 (2002).  
 [2] D. Molnar and M. Gyulassy, Nucl. Phys. A **697**, 495 (2002) [Erratum *ibid.* A **703**, 893 (2002)].  
 [3] Z.W. Lin and C.M. Ko, Phys. Rev. C **65**, 034904 (2002); C.M. Ko, Z.W. Lin and S. Pal, nucl-th/0205056.  
 [4] T.J. Humanic, nucl-th/0205053.  
 [5] J.-Y. Ollitrault, Phys. Rev. D **46**, 229 (1992).  
 [6] S.A. Bass and A. Dumitru, Phys. Rev. C **61**, 064909 (2000).

[7] P.F. Kolb, J. Sollfrank, and U. Heinz, Phys. Rev. C **62**, 054909 (2000).  
 [8] P.F. Kolb et al, Phys. Lett. B **500**, 232 (2001); P. Huovinen et al., Phys. Lett. B **503**, 58 (2001).  
 [9] S. Soff, S.A. Bass, and A. Dumitru, Phys. Rev. Lett. **86**, 3981 (2001); S. Soff, S.A. Bass, D.H. Hardtke, and S.Y. Panitkin, Phys. Rev. Lett. **88**, 072301 (2002).  
 [10] D. Teaney, J. Lauret, and E.V. Shuryak, Phys. Rev. Lett. **86**, 4783 (2001); nucl-th/0110037.  
 [11] T. Hirano, Phys. Rev. C **65**, 011901 (2002).  
 [12] K.H. Ackermann et al. (STAR Collab.), Phys. Rev. Lett. **86**, 402 (2001).  
 [13] C. Adler et al. (STAR Collab.), Phys. Rev. Lett. **87**, 182301 (2001); hep-ex/0205072; nucl-ex/0206001; nucl-ex/0206006.  
 [14] K. Adcox et al. (PHENIX Collab.), nucl-ex/0204005.  
 [15] B.B. Back et al. (PHOBOS Collab.), nucl-ex/0205021.  
 [16] C. Adler et al. (STAR Collab.), Phys. Rev. Lett. **87**, 112303 (2001); **87**, 262302 (2001); Phys. Rev. C **65**, 041901(R) (2002); nucl-ex/0203016; nucl-ex/0205015.  
 [17] K. Adcox et al. (PHENIX Collab.), Phys. Rev. Lett. **88**, 242301 (2002); nucl-ex/0204007;  
 [18] J.M. Burward-Hoy, nucl-ex/0206016; Nu Xu and M. Kaneta, Nucl. Phys. A **698**, 306c (2002).  
 [19] U. Heinz and S.M.H. Wong, Phys. Rev. C, in press [hep-ph/0205051].  
 [20] U. Heinz and P.F. Kolb, Nucl. Phys. A **702**, 269 (2002); hep-ph/0204061.  
 [21] H. Sorge, Phys. Rev. Lett. **78**, 2309 (1997); **82**, 2048 (1999).  
 [22] At late times the fireball parts which have not yet decoupled are already elongated in-plane [7], but the time-integrated source is still extended out-of-plane.  
 [23] S.A. Voloshin and W.E. Cleland, Phys. Rev. C **53**, 896 (1996); Phys. Rev. C **54**, 3212 (1996).  
 [24] U.A. Wiedemann, Phys. Rev. C **57**, 266 (1998).  
 [25] M.A. Lisa, U. Heinz and U.A. Wiedemann, Phys. Lett. B **489**, 287 (2000).  
 [26] U.A. Wiedemann and U. Heinz, Phys. Rept. **319**, 145 (1999); U. Heinz and B.V. Jacak, Ann. Rev. Nucl. Part. Sci. **49**, 529 (1999).  
 [27] U. Heinz, A. Hummel, M.A. Lisa, and U.A. Wiedemann, nucl-th/0207003.  
 [28] P.F. Kolb et al., Nucl. Phys. A **696**, 197 (2001).  
 [29] F. Cooper and G. Frye, Phys. Rev. D **10**, 186 (1974).  
 [30] U.A. Wiedemann and U. Heinz, Phys. Rev. C **56**, 3265 (1997).  
 [31] Z.W. Lin, C.M. Ko and S. Pal, nucl-th/0204054.  
 [32] S. Chapman and U. Heinz, Phys. Lett. B **340**, 250 (1994).  
 [33] P.F. Kolb, J. Sollfrank and U. Heinz, Phys. Lett. B **459**, 667 (1999).  
 [34] H. Heiselberg and A.P. Vischer, Eur. Phys. J. C **1**, 593 (1998);  
 [35] B. Tomášik and U. Heinz, nucl-th/9805016; Acta Phys. Slov. **49**, 251 (1999) [nucl-th/9901006].  
 [36] L. McLerran and S.S. Padula, nucl-th/0205028.  
 [37] C. Adler et al. (STAR Collab.), Phys. Rev. Lett. **87**, 082301 (2001); K. Adcox et al. (PHENIX Collab.), Phys. Rev. Lett. **88**, 192302 (2002).  
 [38] F. Retière et al. (STAR Collab.), nucl-ex/0111013.  
 [39] M. Lisa and R. Wells, unpublished manuscript and private communication.